Correlation Image Velocimetry: A Spectral Approach

Stéphane Roux, François Hild, Yves Berthaud

Correlation Image Velocimetry:

A Spectral Approach

Stéphane Roux

Laboratoire Surface du Verre et Interfaces

UMR CNRS/Saint-Gobain

39 Quai L. Lefranc, F-93303 Aubervilliers Cedex, France

Stephane.Roux@saint-gobain.com

François Hild and Yves Berthaud

LMT-Cachan

ENS de Cachan/CNRS-UMR 8535/Université Paris 6

61 Avenue du Président Wilson, F-94235 Cachan Cedex,

France

Francois.Hild, Yves.Berthaud@lmt.ens-cachan.fr

A new method is introduced to evaluate displacement fields from the analysis of a deformed image as compared to a reference one. In contrast to standard methods, which determine a piecewise constant displacement field, the present method gives a direct access to a spectral decomposition of the displacement field. A minimization procedure is derived and used twice; first, to determine an affine displacement field, then the spectral components of the residual displacement. Although the method is applicable to any space dimension, only cases dealing with one dimensional signals are reported: first, a purely synthetic example is discussed to estimate the intrinsic performance of the method, while a second case deals with a profile extracted from a compressed glass wool sample.

OCIS codes: 070.2590, 100.2000, 100.5010, 120.3940, 120.6150, 040.1520.

1. Introduction

More and more experiments in Solid Mechanics require non-contact strain measurements. In many instances, the possibility to resolve strain inhomogeneities, and thus to determine complete displacement maps becomes highly desirable (e.g., multiphase materials, detection of crack initiation, analysis of singularities [1, 2, 3]). Examples of this may be found in tests being carried out at high temperatures where non contact displacement measurements are necessary. Other applications concern soft solids where strain gages can be difficult to position or may disturb the material's response because of stiffness variations (e.g., glass

wool [4], polymers [5, 6], paper and wood [7]). Let us also mention solids in which strain localization may take place and where inhomogeneous deformation has to be detected to extract reliable information for the identification of a constitutive equation [8].

In recent years, the development of efficient tools for field velocimetry, designed especially in the context of fluid flow visualization [9], has been quite important, and the fast evolving capabilities of digital image acquisition and software for image analysis led us to use such techniques for full-field displacement analysis. Particle Imaging Velocimetry (PIV) [10, 11], Digital Image Correlation (DIC) [2] or more generally Correlation Imaging Velocimetry (CIV) has proven to be an efficient and robust tool whose precision can be extended much below the pixel accuracy (10^{-2} pixel precision and sensitivity is common [12, 13] and in some favorable cases a 10^{-3} precision can be reached [13]). The spirit of the method is to look for the maximum correlation between small zones extracted from the 'deformed' and reference images recorded under different exposures [14]. The translation which corresponds to the maximum correlation can be obtained for different positions of the zone of interest. This allows for the determination of a displacement field which is piecewise constant. The correlations are studied either in the reference space [15, 16, 12] or in Fourier space [17, 18, 19] and the extensive use of Fast Fourier Transforms (FFT) is very effective in reducing the computation cost.

It is tempting to go one step further, and to introduce continuous displacement fields [20, 21]. There is no theoretical problem related to the formulation of such an approach by using finite element discretizations. However, the computation cost increases dramatically since an FFT cannot be used directly. Moreover, the functional to minimize displays many secondary minima, and thus algorithms such as simulated annealing are to be used [22]. This

impacts strongly on the computation cost and convergence may be problematic in practical cases. However, the method clearly provides a much more accurate displacement field [23].

The purpose of the present study is to propose a novel approach based on continuous displacement fields (in Fourier space) which is robust and computationally efficient. The displacement field is obtained from a fast converging iterative procedure where each step requires only two FFTs. After a presentation of the method, two examples of one-dimensional applications are discussed. The first one is a synthetic case where the method can be tested in ideal conditions (no noise nor digitization artefacts). This case shows that the method can deal with strains varying within the range $\pm 25\%$ along the same profile. The second one is based on a real sample (glass wool) uniaxially compressed, where a significant degree of heterogeneity may be present, and where still a one dimensional displacement field is suited.

2. Problem Definition

The surface of a solid has a random heterogeneous texture which is characterized by a grey-level signal (or 'image') called $f(x)$ in its reference state. The 'deformed' image of the same surface is called $g(x)$. The corresponding displacement $u(x)$ is such that $X = x + u(x)$, where X identifies the position in the deformed image of a point x in the reference one. The texture of the surface is assumed not to be affected by the strain, and thus the relation between f and g is postulated to be

$$g(X) = g(x + u(x)) \equiv f(x) \tag{1}$$

Let us note that this kind of hypothesis may be valid for an image obtained from a textured surface observed by reflection. In other instances, such as an image obtained in transmission, the change of the grey level may depend on the local strain, and thus the basic hypothesis (1)

will be violated. However, it will be shown on a practical example that this limitation may still be overcome by the method proposed herein. There may be some additional noise induced by the experimental conditions and the acquisition devices (e.g., readout noise, digitization). The problem to solve is the determination of the unknown displacement field $u(x)$ from the analysis of two signals f and g.

3. Proposed Approach

The Fourier transform $\tilde{g}$ of g can be written as

$$\tilde{g}(k) = \mathcal{F}[g](k) = \int g(X) \exp(2i\pi kX) dX = \int f(x) \exp(2i\pi k[x + u(x)])(1 + u'(x)) dx \quad (2)$$

where $\mathcal{F}[.]$ is the Fourier transform of any function '.' (the dot '.' denotes any dummy parameter or function). Under the hypothesis of small perturbations in the range of considered wavenumbers, i.e., $ku(x) \ll 1$ and $u'(x) \ll 1$, the exponential can be Taylor-expanded up to the first order in $ku(x)$ and $u'(x)$

$$\tilde{g}(k) = \tilde{f}(k) + \int \exp(2i\pi kx) f(x)(u'(x) + 2i\pi k u(x)) dx \quad (3)$$

Integration by parts of Eq. (3) yields

$$\tilde{g}(k) = \tilde{f}(k) - \int \exp(2i\pi kx) f'(x) u(x) dx + [\exp(2i\pi kx) f(x) u(x)]_0^L \quad (4)$$

where the coordinate x ranges from 0 to L. The condition $ku \ll 1$, for a given displacement u, implies that this equation is only valid for small k values. An upper limit k_1 in k space is introduced so that the above expansion is valid. For convenience, a low-pass filter in Fourier space $\tilde{H}_1(k)$ is used

$$\tilde{H}_1(k) = \begin{cases} 1 & \text{if} \quad k \leq k_1 \\ \\ 0 & \text{if} \quad k > k_1 \end{cases} \quad (5)$$

that will be applied to Eq. (4)

$$(\tilde{f}-\tilde{g})(k)\tilde{H}_1(k) = \int \exp(2i\pi kx)\tilde{H}_1(k)f'(x)u(x)dx - \tilde{H}_1(k)[\exp(2i\pi kx)f(x)u(x)]_0^L \qquad (6)$$

Equation (6) is the starting point of the present approach.

A. Periodic Case

Let us first consider a case where both the texture f and the displacement u are periodic so that the bracket in Eqs. (4) and (6) disappears. The treatment of edge effects is discussed in a subsequent section. A simple case is found and it allows us to outline the most important steps of the method. A Fourier decomposition of the trial displacement field U is introduced

$$U(x) = \frac{1}{2\pi}\int_{K\leq K_2} \tilde{U}(K)\exp(-2i\pi Kx)dK \qquad (7)$$

This decomposition defines the space of displacement field in which u will be approximated by U when K is arbitrarily chosen. The range K_2 of K values to be used was not yet specified, but it has to be much smaller than the number of pixels of the original 'image' L. Moreover, since Fourier expressions will be used, the range of k values which can be used will naturally limit the maximum range of K: $K \leq K_2 < k_1$. Equation (6) can be rewritten as

$$(\tilde{f}-\tilde{g})(k)\tilde{H}_1(k) = \int_{K\leq K_2} \tilde{U}(K)\tilde{f}'(k-K)\tilde{H}_1(k)dK \qquad (8)$$

If the power spectrum of $f'U$ is small in the high frequency domain (i.e., high values of k), and if $k_1 \gg K_2$, the integration domain of Eq. (8) can be slightly modified and an approximate solution to the right hand side is

$$(\tilde{f}-\tilde{g})(k)\tilde{H}_1(k) \approx \int_{K\leq K_2} \tilde{U}(K)\tilde{f}'(k-K)\tilde{H}_1(k-K)dK \qquad (9)$$

and the Fourier transform of the image difference between f and g is simply the convolution of the Fourier transform of the displacement by the signal gradient. An inverse Fourier transformation shows that Eq. (8) can be seen as a Taylor expansion of Eq. (1)

$$g(x) \approx f(x - U(x)) \approx f(x) - f'(x)U(x) \tag{10}$$

However, this expansion is generally of little use. The texture is a random function with rapidly varying grey levels, so that the above expression would only be valid for extremely small displacements. Otherwise, trying to use this direct expression will lead to inaccurate results, because of the existence of spurious local solutions. To consider this kind of approach, a low pass filtering (i.e., convolution by H_1) has to be performed to ensure that the Taylor expansion up to the first order may be of any use. Therefore, the advantage of working directly in Fourier space appears naturally.

There are now different strategies one could follow to use Eq. (9). The first one is to derive a weak formulation in such a way that as many equations as unknowns are obtained. The second one, which gives less freedom in the choice of the weak formulation, is to write the problem in terms of the minimization of a functional of the unknown displacement.

B. Weak Formulation

Let us consider the convolution of Eq. (9) by $\tilde{f}'\tilde{H}_1$. For any value K', one can write

$$\int_k (\tilde{f} - \tilde{g})(k)\tilde{H}_1(k)\tilde{f}'(K' - k)\tilde{H}_1(K' - k)dk =$$
$$= \int_{K \leq K_2} \tilde{U}(K) \int_k \tilde{f}'(k - K)\tilde{H}_1(k - K)\tilde{f}'(K' - k)\tilde{H}_1(K' - k)dkdK \tag{11}$$

Convolution in Fourier space being Fourier transforms of direct product in real space, the above equation can be rewritten as

$$\widehat{(f-g)}(x)\hat{f}'(x) = U(x)\hat{f}'^2(x) \tag{12}$$

where $\hat{(.)}$ is the filtering of $(.)$ obtained by convolution with H_1. Equation (12) is formally identical to Eq. (10). A direct expression for the trial displacement field $U(x)$ is

$$U(x) = \frac{\widehat{(f-g)}(x)\hat{f}'(x)}{\hat{f}'^2(x)} \tag{13}$$

Even though Eq. (13) could be simplified and would be identical to Eq. (10), it is more convenient to keep the present formulation that can be generalized to 2D situations [24]. The above formula again appears very attractive, because of the direct expression of the displacement field. Yet some care has to be exercised in the precise implementation of this equation in a code. In regions where $\tilde{f}'$ vanishes, the above ratio becomes ill-behaved. This phenomenon is to be expected since a displacement cannot be determined for a signal of constant level.

The range of K values to be used was not specified. Intrinsically, the minimum wavelength of u to be determined has to be greater than the correlation length of the initial texture. This is an unavoidable constraint that cannot be overcome. There is a secondary limitation due to the followed derivation, i.e., the hypothesis that ku be small. This means in practice that only small $k \leq k_1$ values are to be used, and therefore only long wavelength displacements $K \leq k_2 < k_1$ can be resolved. However, this constraint can be overcome since one can proceed recursively. First, only the long wavelength modes should be determined by using a small number of Fourier modes for u. Once this first low band displacement field has been determined, one can reconstruct a modified g image corrected by this first

displacement. Then, the amplitude of the residual displacement is expected to be reduced significantly. This means that the same procedure can be used again with a somewhat larger range of wavenumbers in this second stage to determine a more accurate displacement field. Recursive use of this technique is thus expected to be able to provide accurate displacement fields.

C. Minimization

An alternative route is to formulate the problem in terms of a minimization of a functional of trial displacement fields, U. For convenience, the adjoint $\underline{U}$ is preferred and defined such that if $X = x + U(x)$, then $x = X - \underline{U}(X)$. For small displacements, a first order approximation is $\underline{U}(x) \approx U(x)$. Let us introduce the functional $\mathcal{A}$

$$\mathcal{A}[\underline{U}] = \int (g(X) - f(X - \underline{U}(X)))^2 dX \tag{14}$$

or in Fourier space, by using Parseval's theorem

$$\mathcal{A}[\underline{U}] = \int \left| \tilde{g}(k) - \mathcal{F}[f(. - \underline{U}(.))](k) \right|^2 dk \tag{15}$$

If the unknown displacement field is assumed to be constant, i.e., $\underline{U}(X) = \underline{V}$, minimizing the functional $\mathcal{A}[\underline{V}]$ is strictly equivalent to maximizing the functional $\mathcal{H}(\underline{V})$

$$\mathcal{H}(\underline{V}) = \int g(X) f(X - \underline{V})\ dX \tag{16}$$

where $\mathcal{H}$ is the cross-correlation product of the two signals. The use of an FFT speeds up the computations of the cross correlation product. Equation (16) constitutes the basis of all CIV techniques [14]. When some noise is added between the two signals, it can be shown that the previous estimate is optimum for a white noise.

Moreover, since the high frequency part of the above signal is expected to contain more noise than information, the functional $\mathcal{A}$ is restricted to a limited range of k values and is denoted by $\widehat{\mathcal{A}}$

$$\widehat{\mathcal{A}}[\underline{U}] = \int \left| \tilde{g}(k) - \mathcal{F}[f(. - \underline{U}(.))](k) \right|^2 \tilde{H}_1(k) dk \tag{17}$$

The trial displacement field $\underline{U}$ is written in a spectral form over a limited range of wavenumbers, $\underline{U} = \frac{1}{2\pi} \int_{K \leq K_2} \tilde{U}(K) \exp(-2i\pi Kx) dK$. By assuming a periodic case and proceeding along the same lines as in Eq. (9), the following estimate is obtained for low values of k

$$\mathcal{F}[f(. - \underline{U}(.))](k) = \tilde{f}(k) - \int_{K \leq K_2} \tilde{U}(K) \tilde{f}'(k - K) \tilde{H}_1(k - K) dK \tag{18}$$

Thus the functional $\widehat{\mathcal{A}}$ reads

$$\widehat{\mathcal{A}}[\underline{U}] = \int \left| (\tilde{g} - \tilde{f})(k) - \int_{K \leq K_2} \tilde{U}(K) \tilde{f}'(k - K) \tilde{H}_1(k - K) dK \right|^2 \tilde{H}_1(k) dk \tag{19}$$

where $\widehat{\mathcal{A}}$ is a quadratic form in the unknowns $\tilde{U}(K)$, and thus expressing the condition to be fulfilled at the minimum is straightforward. By neglecting the power corresponding to high frequencies of fU, the following linear system has to be solved

$$\begin{aligned} \int_{K' \leq K_2} \tilde{U}(K') \int_k \tilde{f}'(K - k) \tilde{H}_1(K - k) \tilde{f}'(k - K') \tilde{H}_1(k - K') dk dK' = \\ = \int_k (\tilde{f} - \tilde{g})(k) \tilde{H}_1(k) \tilde{f}'(K - k) \tilde{H}_1(K - k) dk \end{aligned} \tag{20}$$

One can recognize the same system as in the previous section (Eq. (11)). This legitimates the choice of the weak formulation. The present approach is thus expected to be well-behaved since it relies on the existence of a well-defined minimum, the quality of which can be further estimated by computing $\widehat{\mathcal{A}}$.

4. Edge Effects

The proposed method relies heavily on the properties of Fourier transforms, and the interplay between convolution in direct and reciprocal spaces leads to convenient numerical implementation. However, the drawback is that all functions are implicitly assumed to be periodic. This may cause some problems on the edges. In particular, a non zero average strain implies that the physical length is different in the reference and deformed images. This point cannot be accounted for in the basis of selected functions.

A natural way to circumvent this problem is first to adjust the correct physical scales in both images in such a way that the mean strain is zero in the rescaled coordinates. To comply with the approach presented so far, the displacement field is defined by $\underline{W}(x) = a_2 x + a_1$. The functional to minimize becomes

$$\mathcal{A}[\underline{W}] = \int \left((g-f)(x) - \underline{W}(x) f'(x)\right)^2 dx \tag{21}$$

where $g-f$ and f' have to be conveniently filtered before such a formula may be applicable. In practice, a very severe initial filtering is first performed, and progressively more and more Fourier modes are incorporated (see Section 5).

The simple form chosen for $\underline{W}$ yields a very simple minimization condition that can be written in matrix form

$$\mathbf{M}\mathbf{A} = \mathbf{B} \tag{22}$$

where

$$\mathbf{A} = \begin{pmatrix} a_1 \\ \\ a_2 \end{pmatrix} \tag{23}$$

and similarly for the components of the matrix $\mathbf{M}$ and $\mathbf{B}$, whose explicit components are

$$M_{ij} = \int \widehat{f'}^2(x) x^{i+j-2} dx \tag{24}$$

and

$$B_i = \int (\widehat{f - g})(x) \widehat{f'}(x) x^{i-1} dx \tag{25}$$

where i and j indices range from 1 to 2. As previously mentioned, in these expressions, f' and $f - g$ are to be filtered prior to the computation of the integrals.

5. Test of the Method on an Artificial Case

The proposed method is first applied on an artificially generated example. The texture itself is first generated by using a random walk. Periodic boundary conditions are prescribed by subtracting the end-to-end linear drift, so that the two end points of the profile correspond to the same 'grey level', $f(0) = f(L)$. A random displacement field is chosen arbitrarily in Fourier space so that a periodic boundary condition is automatically set. The number of modes is chosen to be equal to 30, with a Gaussian distributed random amplitude and phase. An overall translation (mode $k = 0$) is also prescribed. From the reference texture and the displacement field, the deformed image, g, is generated by using a linear interpolation of f. The typical amplitude of the difference between maximum and minimum displacement could reach values as high as 30 pixels. The maximum local strain is equal to 25% in this particular example. Figure 1 shows a typical example of the reference and deformed texture. The number of pixels used in the definition of the texture is 1024. The program that generates such artificial cases is designed to be totally independent of the analysis program.

The analysis is divided into different steps. The first one consists in determining an

affine displacement field, which is a first coarse estimate of the actual displacement field. It is based on the procedure outlined in Section 4. For each iteration i, more and more Fourier modes of the two signals are added. It is found that $k_1(i) = 5 + 12 \times i$ is a good choice. This first step stops when Root Mean Square (RMS) of the signal difference no longer decreases. In the present example, 8 iterations are used. Due to the periodicity of the profile and of the displacement field, there is no need to compute the mean strain since the latter should vanish. If one turns off this part of the computation, the convergence is faster. However, since typical cases are not periodic, the treatment was not specialized to such cases.

The second part consists in determining Fourier modes of the displacement field. The procedure is now based on the direct application of the method discussed in Section 3. This time, two parameters are important, namely the values k_1 and K_2 of the filters. For each iteration $j \geq 1$, $k_1(j) = 301 + 14 \times (j-1)$ and $K_2(j) = 15 + 2 \times (j-1)$. The convergence criterion consists in looking for the minimum RMS error of the signal difference $f - g$ where g is computed as a function of the transformed coordinates so that if the displacement were exactly determined, f and g would fall on top of each other. It is important to stress that the iterative calls to the main procedure with an increasing number of Fourier modes is the best way to achieve a good accuracy of the method since the previously determined displacement field is used to modify the reference profile in the rescaled coordinates. Therefore the residual displacement becomes smaller and smaller in amplitude and leads to a good convergence. A direct call to the main procedure asking for, say, 30 Fourier modes would not give such a faithful determination of the displacement field. Figure 2 shows this effect. The first iterations are used to evaluate the affine part of the displacement. Due to periodicity of the prescribed displacement, no significant decrease can be seen. The subsequent iterations correspond to

the computation of the spectral decomposition. A gradual decrease of the error is found. The last iteration is that for which the RMS error reaches its minimum value; 41 iterations are required in the present case.

The final displacement field is compared to the prescribed one. A quasi-perfect agreement is found apart from some remaining edge effects (Fig. 3). The latter effect is due to the initial determination of the mean translation and strain (Section 4) which does not assume implicitly the periodicity of the fields. The difference in terms of a Root Mean Square (RMS) measure of the displacement difference is equal to 7×10^{-3} pixel when the first and last 80 pixels of the signal are not considered (average displacement: 12.8 pixels and standard deviation 7.55 pixels). By omitting the first step of the analysis gives better (quasi-perfect) results in the particular case of a periodic signal, with a periodic displacement field. The conclusion derived from this observation is that edge effects still constitute a weak point of the method (as for all other methods), and some more effort should be devoted to their analysis.

6. Test on a Real Case

The above test is quite satisfactory, however, by construction there is no noise in the signal, and more importantly, the basic hypothesis (1) is met. However, in real cases, this assumption is only roughly satisfied, in particular when the images are obtained in transmission mode. There is always a slight shift in contrast and in light intensity which may affect the overall efficiency. Furthermore, by construction, CCD cameras produce noise (e.g., photon noise, readout noise, dark current noise). Lastly, the signal is digitized thereby limiting the minimum detectable displacement [13]. Therefore it is important to test the method by using realistic signals. The real displacement field is unknown, and a direct evaluation of the

method is impossible. To get some insight into the accuracy of the proposed approach, a comparison with another tool developed for the same goal is chosen, i.e., an independent code based on the maximization of the cross-correlation of two zones is developped, by assuming a single translation of each zone (see Eq. (16)). This method, usually referred to as Correlation Imaging Velocimetry, or CIV, is very widespread in the field of Fluid Mechanics for field determination of velocities [25] and has become popular in Solid Mechanics to evaluate displacement and strain fields [2]. In practice, an implementation of this method (CORRELI^{1D}) is developed in Matlab^{TM} [26, 13].

The case used to test the method is a $140 \times 200 \times 50$ mm^3 sample of glass wool, which in its deformed state is uniaxially compressed by about 3%. The advantage of this system is that it has a rather heterogeneous natural texture for which images are obtained in transmission with no special preparation (Fig. 4). Out-of-plane displacements remain vanishingly small, therefore no correction is made in the present study [28]. Moreover, due to the structure of the medium, the displacement field is essentially along the main contraction axis, and hence it is well-suited to the one-dimensional analysis proposed in this study. The rather loose structure also induces large strains while still preserving an elastic (although non-linear) behavior [27].

Figure 5 gives an example of the two profiles f and g obtained from the glass wool sample. The program used in this section is the same as in the previous one. Figure 6 shows the result of the analysis, through the direct comparison of the profiles (deformed versus reference one in rescaled coordinates), and the resulting difference. As judged from this plot, the method allows one to erase most of the difference in the two images. The difference expressed as a Root Mean Square (RMS) measure is equal to 2.9 in terms of grey level for

a texture with a standard deviation of 35.2 and an average of 142. It can be noted that this value is only an *indication* (i.e., an upper bound) of the error of the method since it also incorporates other sources related to the CCD camera as well as the experiment itself, which induces a variation of grey level due to the contraction of the specimen and the fact that the images are obtained in transmission.

Figure 7 shows the displacement profile obtained with the present technique and compared to the result of a DIC method. In the latter case, the size of the Zone of Interest (ZOI), for which each correlation estimate is performed, was chosen to be 64 pixels. To have a more extensive determination of the displacement field, the estimate of the displacement field is computed by placing the center of the ZOI successively at every point of the image after omitting 20 pixels at each end. This gives a rather continuous curve, although it is not representative of the true resolution since the ZOI size is still quite large. A smaller ZOI (i.e., 32 pixels) resulted in a much noisier displacement field, and was discarded. The short wavelength fluctuation in the determined displacement field is most probably due to intrinsic limitations of the method rather than real fluctuations. To obtain such a result, the first step of the procedure (i.e., determination of an affine displacement field) is required, otherwise the optimum displacement is trapped in spurious very remote local minima, and the result is difficult to analyze. One can note that such a first correction is naturally implemented in the proposed spectral method without having to carry out by hand such determination. The comparison of the two methods is quite good, although the exact displacement field is unknown. Both results are subjected to their own filtering and sensitivity. The fact that they both agree on most of the available range of data is however, to our opinion, a convincing evidence of the practical interest of *both* methods and their ability to deal with real images.

As a direct probe of the first determination of the affine displacement field as discussed in Section 4, Fig. 8 shows the result of a few (i.e., 8) iterations for the determination of a constant strain field equal to 3%.

The method is a priori not tolerant to differences in grey levels such that the basic hypothesis (1) is violated. To make it more robust, an additional procedure is added to allow for grey level corrections. Once the displacement is determined by using K_2 Fourier modes, the difference $f - g$ is filtered by using at most K_2 Fourier modes and the reference profile f is corrected by the resulting filtered difference. Note that it is important not to use more modes in this correction than in the displacement determination. This same step was also implemented in the program used in the previous section. In the latter case, this procedure should not be relevant, but it was important to test that it does not prevent convergence toward the actual solution.

7. Conclusion

A novel procedure is introduced to determine displacement fields from the comparison of two 'images' in one dimension. It is based on a general minimization scheme that is applied twice; first to estimate an affine displacement field, second to evaluate a truncated spectral decomposition of the residual displacement field. The method has been tested on two cases. A first artificial example where a random texture has been deformed by using a random displacement field, and a second based on real profiles extracted from a compressed glass wool sample. Both cases give accurate estimates of the displacement field when compared either to a known displacement (first example) or to a classical analysis based on DIC (second example).

Extensions of the present method to two dimensional images should be straightforward although it has not been implemented yet. It can be noted that special care should be taken to properly account for edge effects. Furthermore, the filtering process needs to be optimized to treat these new cases. Even though some attention was paid in the present examples, an optimum procedure was not sought and may depend on the spectral content of the texture of the analyzed images as well as that of the displacement fields.

The present method was also used to measure velocities in a turbulent flow by recording of tracer concentrations along one line (by using a laser beam). This method turned out to be quite successful [25] in that case, which underlines the potential interest of the method (even in one dimension), to a wide variety of applications, both in Solid and Fluid Mechanics.

Acknowledgments

The authors wish to acknowledge useful discussions with M. Baudequin, E. Bouzereau, F. Cantelaube, E. Gaudin and J.E. Wesfreid.

References

1. A. Lagarde, ed., *Proc. IUTAM Symposium on Advanced Optical Methods and Applications in Solid Mechanics*, Solid Mechanics and its Applications **82**, (Kluwer, Dordrecht, the Netherlands, 2000).

2. M.A. Sutton, S.R. McNeill, J.D. Helm and Y.J. Chao "Advances in Two-Dimensional and Three-Dimensional Computer Vision," in *Photomechanics*, P.K. Rastogi, ed., Topics in Appl. Phys. **77**, pp. 323-372, (2000).

3. L. Humbert, V. Valle and M. Cottron "Experimental Determination and Empirical Representation of Out-of-Plane Displacements in a Cracked Elastic Plate Loaded in Mode I," Int. J. Solids Struct. **37**, pp. 5493-5504, (2000).

4. M. Baudequin, F. Hild, B. Raka and S. Roux "Strain Field Measurements of Compressed Glass Wool Samples," work in progress, (2000).

5. C. G'Sell, J.-M. Hiver, A. Dahnoun and A. Souahi "Video-Controlled Tensile Testing of Polymers and Metals Beyond the Necking Point," J. Mat. Sci. **27**, pp. 5031-5039 (1992).

6. L. Chevalier, S. Calloch, F. Hild and Y. Marco "Digital Image Correlation used to Analyze the Multiaxial Behavior of Rubber-Like Materials," Eur. J. Mech. A/Solids **20**, pp. 169-187 (2001).

7. D. Choi, J.L. Thorpe and R. Hanna "Image Analysis to Measure Strain in Wood and Paper,"

Wood Sci. Technol. **25**, pp. 251-262 (1991).

8. J. Desrues, J. Lanier and P. Stutz "Localization of the Deformation in Tests on Sand Sample," Engng. Fract. Mech. **21** (4), pp. 909-921, (1985).

9. W. Merzkirch, *Flow Visualization* (Academic, New York, USA, 1987).

10. T.D. Dudderar and P.G. Simpkins "Laser Speckle Photography in a Fluid Medium," Nature **270**, pp. 45, (1977).

11. C.J.D. Pickering and N.A. Halliwell "Speckle Laser in Fluid Flows: Signal Recovery with Two-Step Processing," Appl. Opt. **23**, pp. 1129 (1984).

12. S. Mguil, F. Morestin and M. Brunet "Mesure des déformations par corrélation directe d'images numériques," in *"Photomécanique 98"* (GAMAC, Paris, France, 1998), pp. 361-368 (in French).

13. F. Hild, J.-N. Périé and M. Coret, *Mesure de champs de déplacements 2D par corrélation d'images numériques : CORRELI*^{2D}, Internal Report, LMT-Cachan (in French), **230** (1999).

14. P.K. Rastogi, ed., *Photomechanics*, Topics in Appl. Phys. **77**, (2000).

15. M.A. Sutton, W.J. Wolters, W.H. Peters, W.F. Ranson and S.R. McNeill "Determination of Displacements Using an Improved Digital Correlation Method," Im. Vis. Comp. **1** (3), pp. 133-139 (1983).

16. T.C. Chu, W.F. Ranson, M.A. Sutton and W.H. Petters "Applications of Digital-Image-Correlation Techniques to Experimental Mechanics," Exp. Mech. **3** (25), pp. 232-244 (1985).

17. D.J. Chen, F.P. Chiang, Y.S. Tan and H.S. Don, "Digital Speckle-Displacement Measurement Using a Complex Spectrum Method," Appl. Opt. **32**, pp. 1839, (1993).

18. Y. Berthaud, J. Scholz and J. Thesing, "Méthodes optiques et acoustiques de mesures des caractéristiques mécaniques," in *Proc. Colloque national MECAMAT "Mécanismes et mécanique des grandes déformations*," (in French) pp. 77-80 (1996).

19. F.P. Chiang, Q. Wang and F. Lehman, "New Developments in Full-Field Strain Measurements Using Speckles," in *Non-Traditional Methods of Sensing Stress, Strain and Damage in Materials and Structures* **ASTM STP 1318**, pp. 156, (1997).

20. H. Huang, H. Fiedler and J. Wang, "Limitation and Improvement of PIV; Part I: Limitation of Conventional Techniques due to Deformation of Image Patterns," Exp. Fluids **15**, pp. 168-174, (1993).

21. H. Huang, H. Fiedler and J. Wang, "Limitation and Improvement of PIV; Part II: Particle Image Distorsion, a Novel Technique," Exp. Fluids **15**, pp. 263-273, (1993).

22. W.H. Press, S.A. Teukolsky, W.T. Vetterling and B.P. Flannery, *Numerical Recipes* (Cambridge University Press, Cambridge, USA, 1992).

23. P. Tokumaru and P. Dimotakis, "Image Correlation Velocimetry," Exp. Fluids **19**, pp. 1-15,

(1995).

24. B. Wagne, S. Roux and F. Hild, "Determination of 2D Displacement fields by a Spectral Approach," work in progress (2001).

25. E. Bouzereau, *A Review of Imaging Velocimetry Methods*, Internal Report, ENSTA (2000).

26. Matlab^{TM} 5.3. The MathWorks, inc., http://www.mathworks.com (1999).

27. M. Baudequin, G. Ryschenkow and S. Roux, "Non-Linear Elastic Behavior of Light Fibrous Materials," Eur. Phys. J. B **12**, pp. 157-162, (1999).

28. P. Jacquot and P.K. Rastogi "Influence of Out-of-Plane Deformation and its Elimination in White Light Speckle Photography," Opt. Lasers Eng. , pp. 33-55 (1981).

List of Figures

Figure 1: Two artificial textures f (dashed line) and g (solid line) as generated from a random walk.

Figure 2: Change of the RMS error in displacement with the number of iterations. The first 8 iterations correspond to the affine estimate of the displacement field. The subsequent 41 iterations are used to evaluate the Fourier modes of the displacement field.

Figure 3: The solid line shows the prescribed displacement (defined by using 30 Fourier modes), while the dashed line is the estimate obtained from the present method after 8 + 41 iterations (i.e., 95 Fourier modes). Note that the only significant error (bottom curve) between the prescribed and computed displacement field is confined on the edges of the signal.

Figure 4: Schematic of the experimental set-up. The Region Of Interest (ROI) is acquired initially and after various contractions. Example of reference and deformed pictures of a glass wool sample (1008×1016 pixels, 8-bit digitization).

Figure 5: Two functions f (dashed line) and g (solid line) as measured on the reference and the deformed sample of glass wool.

Figure 6: Superimposed profiles f (dashed line) and g (solid line) accounting for the dis-

placement field as determined by using 55 Fourier modes. The bottom line corresponds to the difference $f - g$, i.e., an estimate of the error.

Figure 7: Displacement field estimated from the present method (solid line), using 55 Fourier modes for the glass wool sample (8+21 iterations) compared with the result of a DIC analysis with a ZOI of size 64 pixels (dashed line), which is totally independent.

Figure 8: First determination of an affine displacement field (solid line) using the first treatment discussed in Section 4 (8 iterations). For comparison purposes, the displacement field (dashed line) is shown and is determined by a standard DIC technique, which is totally independent.

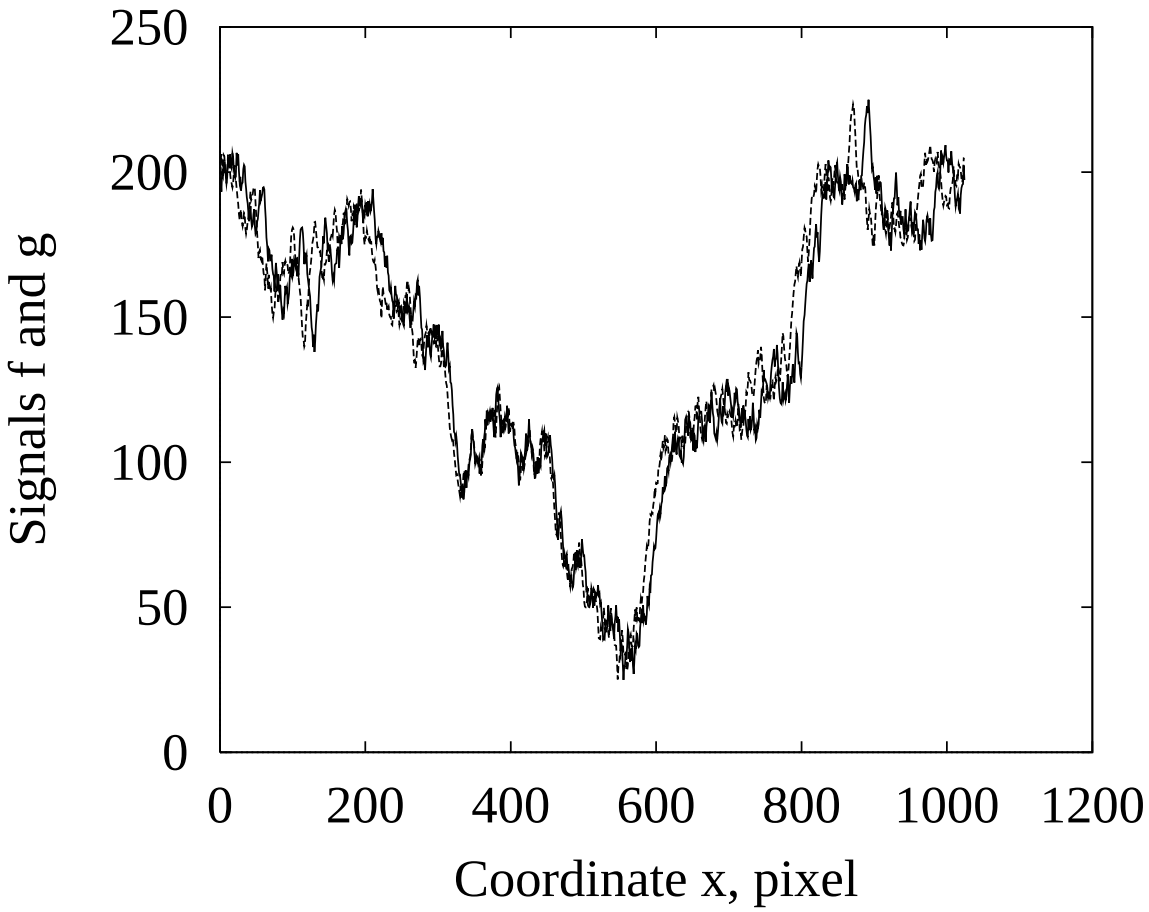

Fig. 1. Two artificial textures f (dashed line) and g (solid line) as generated from a random walk.

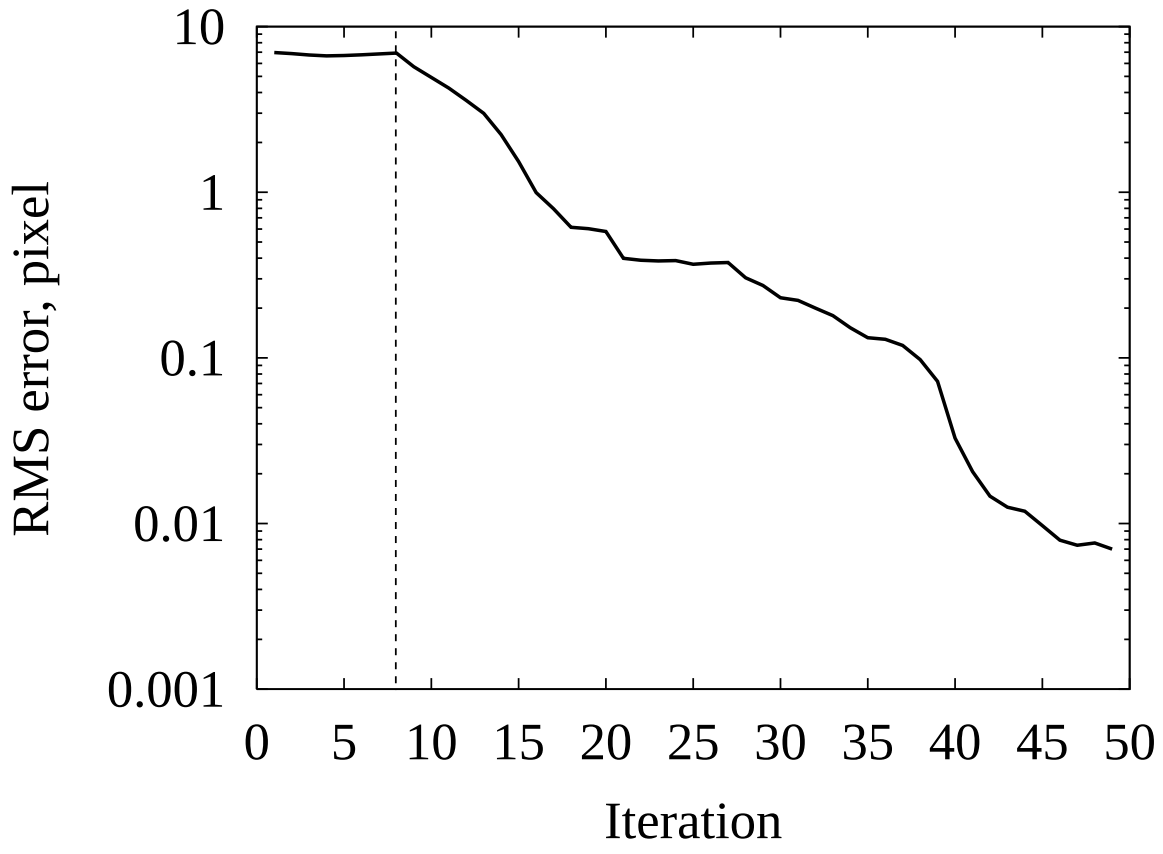

Fig. 2. Change of the RMS error in displacement with the number of iterations. The first 8 iterations correspond to the affine estimate of the displacement field. The subsequent 41 iterations are used to evaluate the Fourier modes of the displacement field.

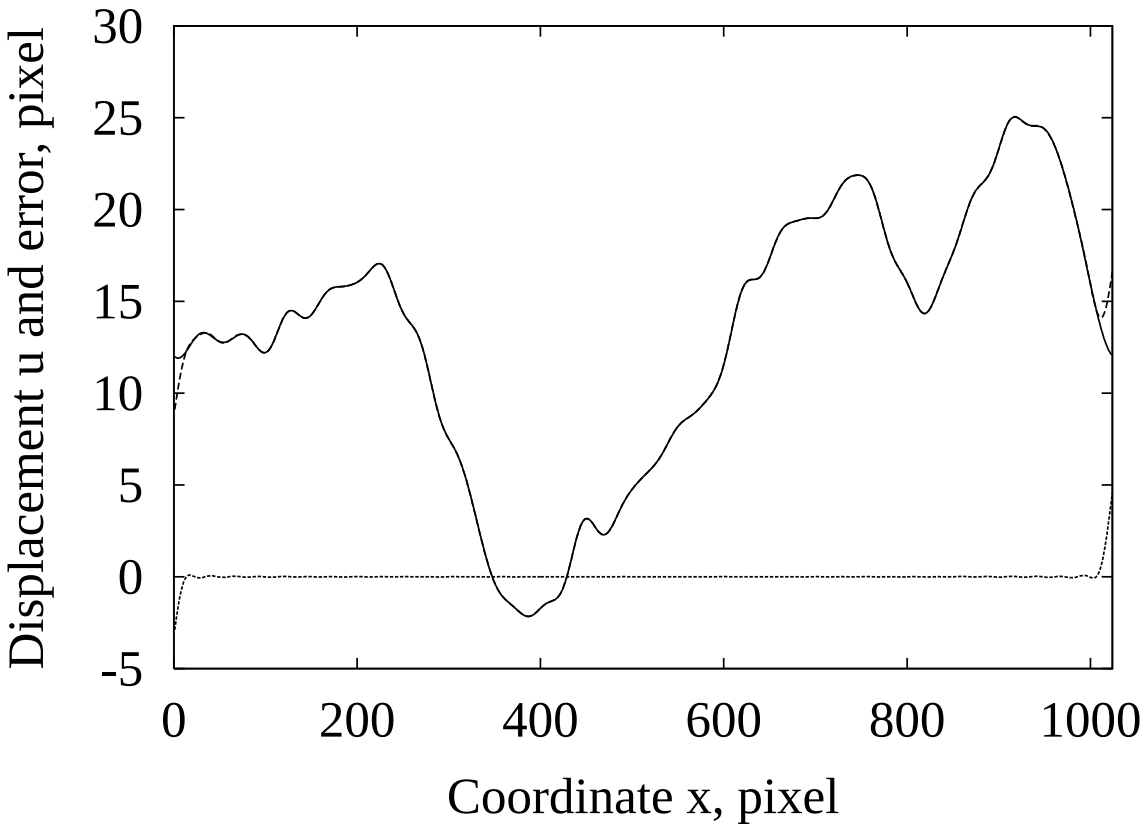

Fig. 3. The solid line shows the prescribed displacement (defined by using 30 Fourier modes), while the dashed line is the estimate obtained from the present method after 8 + 41 iterations (i.e., 95 Fourier modes). Note that the only significant error (bottom curve) between the prescribed and computed displacement field is confined on the edges of the signal.

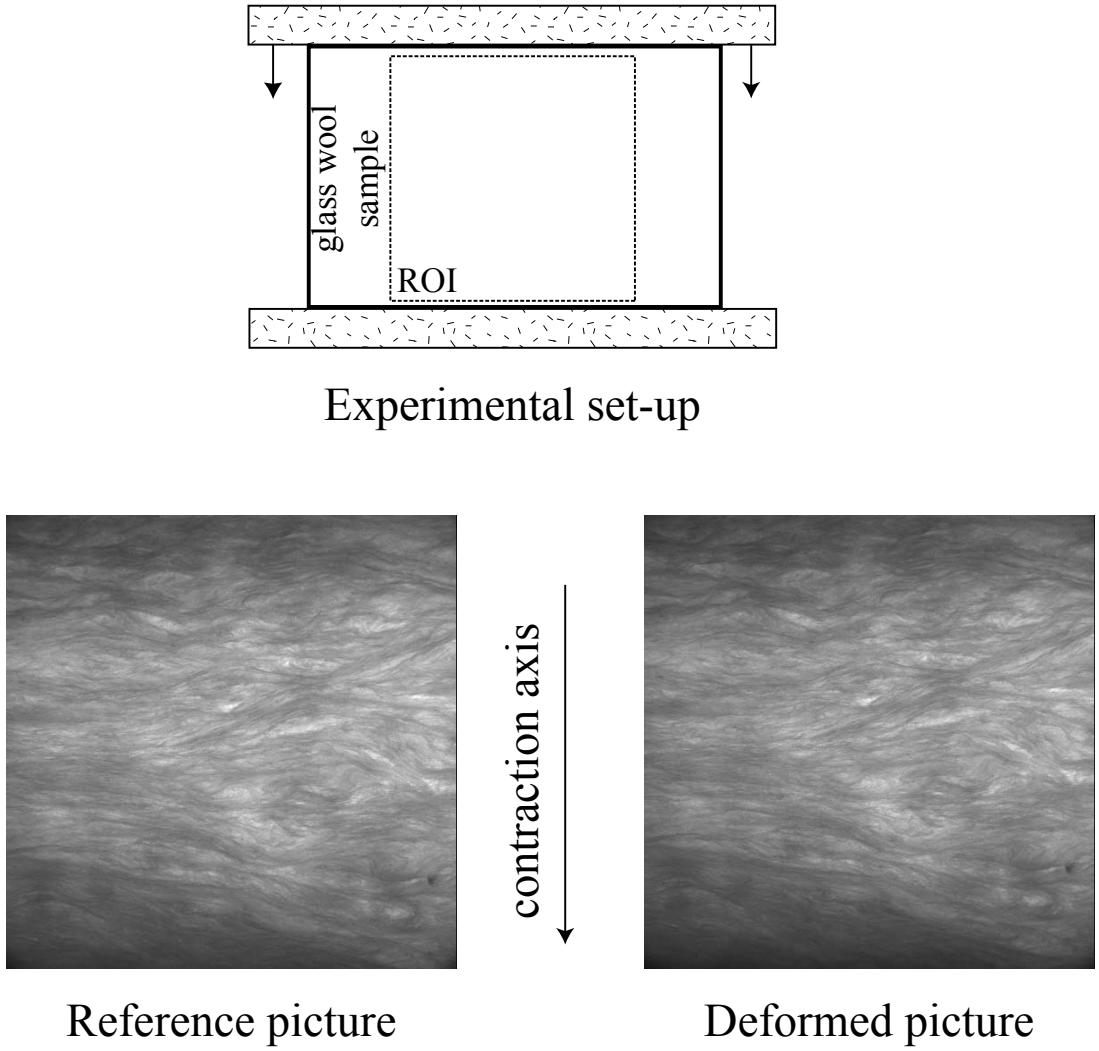

Fig. 4. Schematic of the experimental set-up. The Region Of Interest (ROI) is acquired initially and after various contractions. Example of reference and deformed pictures of a glass wool sample (1008 $\times$ 1016 pixels, 8-bit digitization).

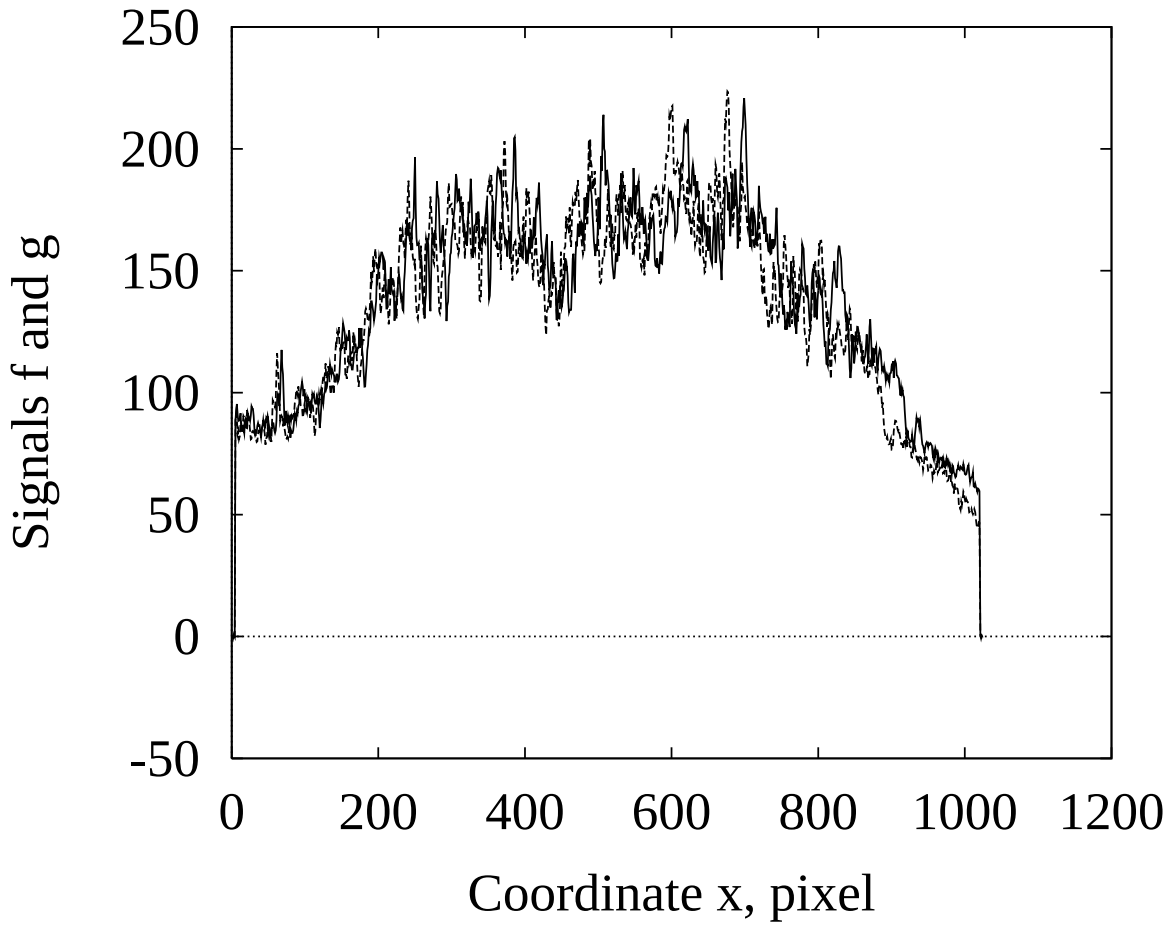

Fig. 5. Two functions f (dashed line) and g (solid line) as measured on the reference and the deformed sample of glass wool.

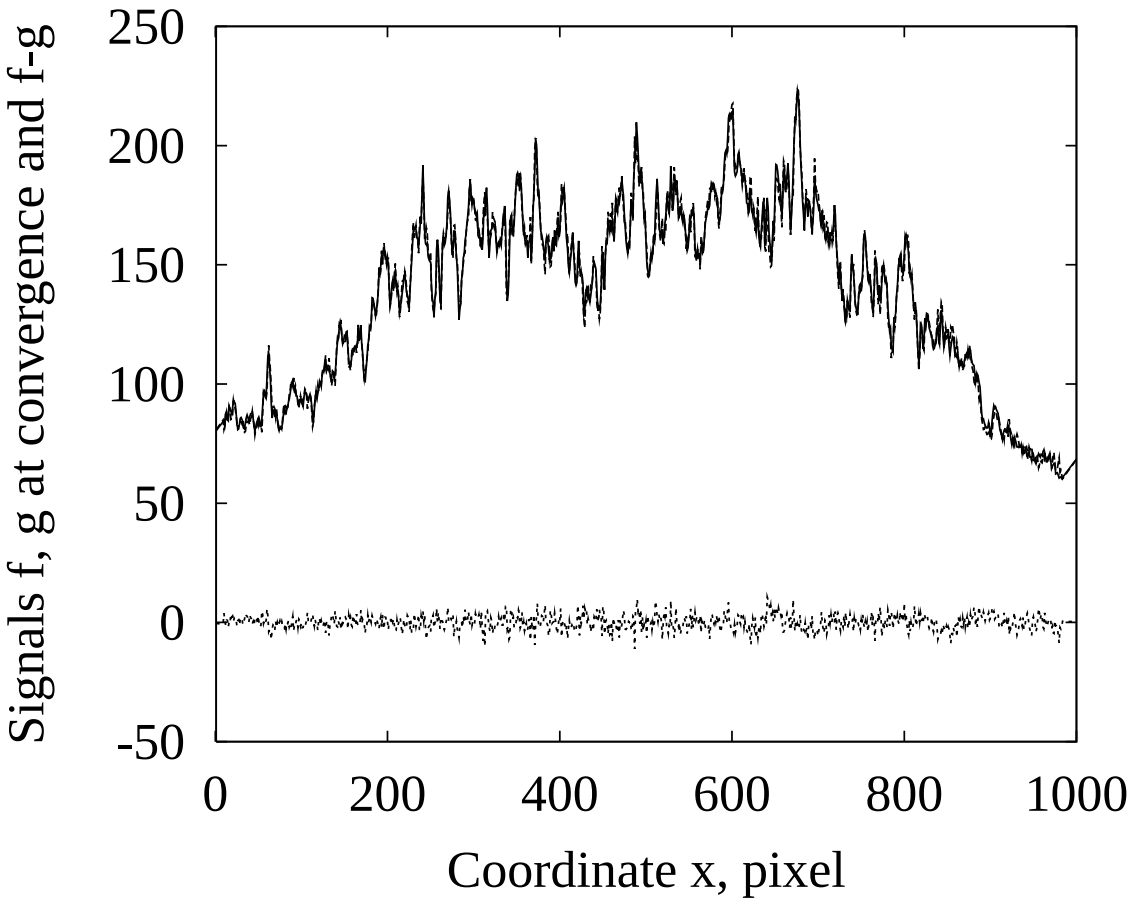

Fig. 6. Superimposed profiles f (dashed line) and g (solid line) accounting for the displacement field as determined by using 55 Fourier modes. The bottom curve corresponds to the difference $f - g$, i.e., an estimate of the error.

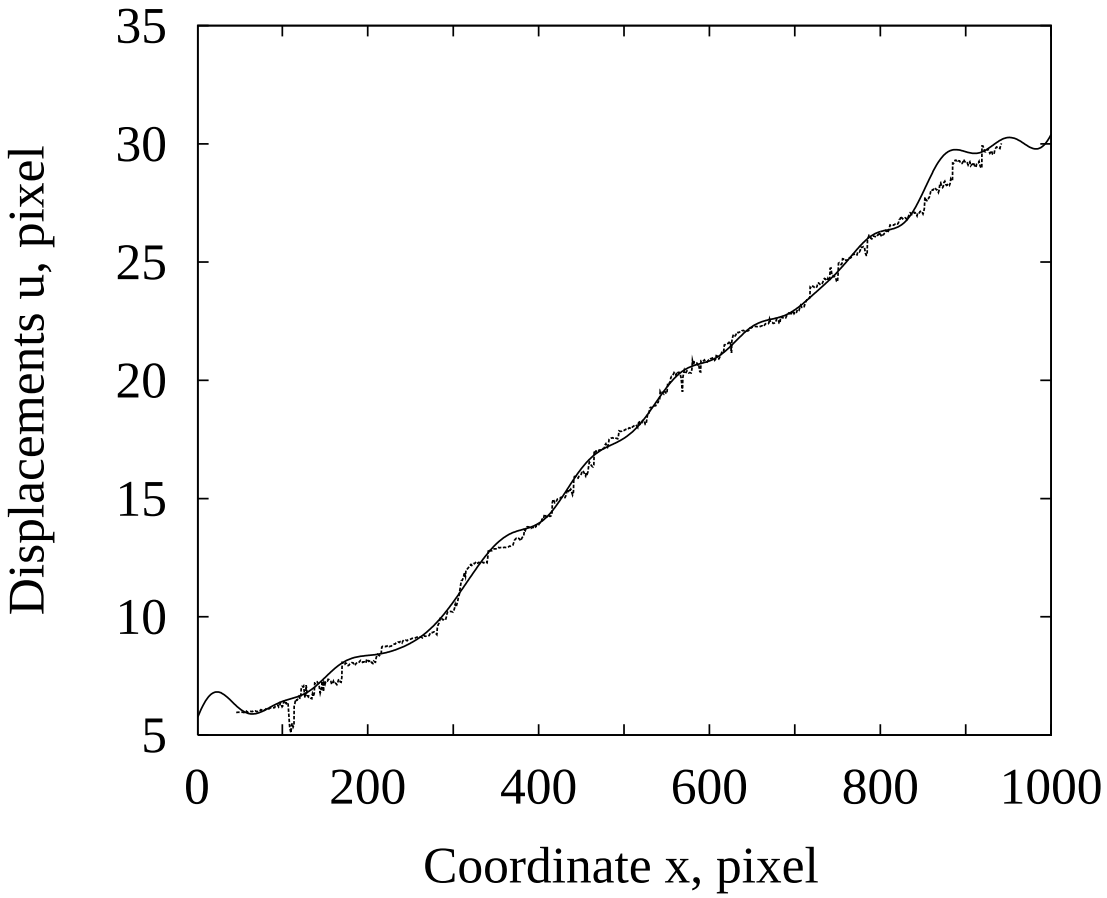

Fig. 7. Displacement field estimated from the present method (solid line), using 55 Fourier modes for the glass wool sample (8+21 iterations) compared with the result of a DIC analysis with a ZOI of size 64 pixels (dashed line), which is totally independent.

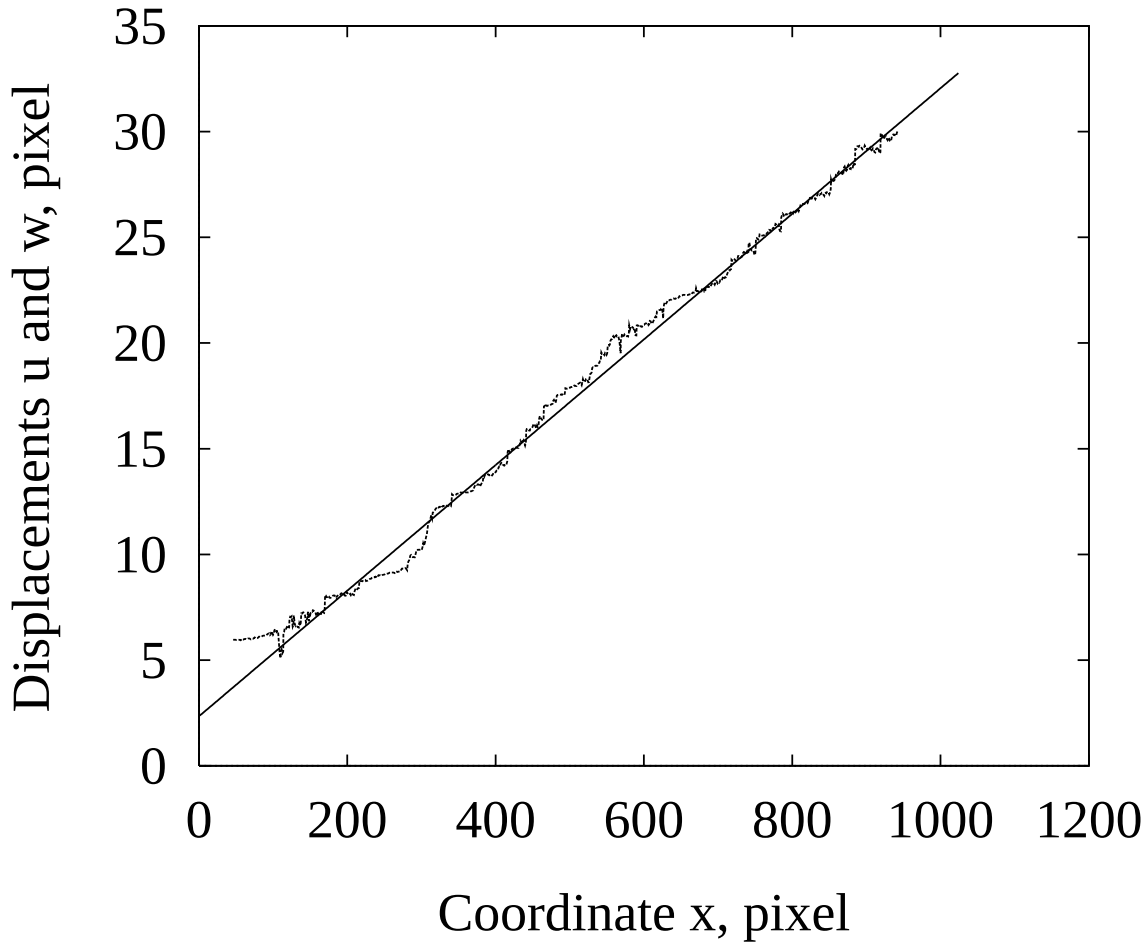

Fig. 8. First determination of an affine displacement field (solid line) using the first treatment discussed in Section 4 (8 iterations). For comparison purposes, the displacement field (dashed line) is shown and is determined by a standard DIC technique, which is totally independent.